

NASA TECHNICAL MEMORANDUM 100494  
USAAVSCOM TECHNICAL MEMORANDUM 87-B-12

STRAIN-ENERGY-RELEASE RATE ANALYSIS  
OF THE END-NOTCHED FLEXURE SPECIMEN  
USING THE FINITE-ELEMENT METHOD

P. 33

S. A. Salpekar, I. S. Raju, and T. K. O'Brien

(NASA-TM-100494) STRAIN-ENERGY-RELEASE RATE  
ANALYSIS OF THE END-NOTCHED FLEXURE SPECIMEN  
USING THE FINITE-ELEMENT METHOD (NASA)  
33 p Avail: NTIS HC A03/MF A01 CSCL 20K

N88-13735

Unclas  
G3/39 0111863

NOVEMBER 1987



National Aeronautics and  
Space Administration

Langley Research Center  
Hampton, Virginia 23665

**STRAIN-ENERGY-RELEASE RATE ANALYSIS OF THE END-NOTCHED  
FLEXURE SPECIMEN USING THE FINITE-ELEMENT METHOD**

S. A. Salpekar\*, I. S. Raju\*, and T. K. O'Brien\*\*  
NASA Langley Research Center  
Hampton, Virginia 23665-5225

**SUMMARY**

Two-dimensional finite-element analysis of the end-notched flexure specimen was performed using 8-node isoparametric, parabolic elements to evaluate compliance and mode II strain-energy-release rates,  $G_{II}$ . The  $G_{II}$  values were computed using two different techniques: the virtual crack-closure technique (VCCT) and the rate of change of compliance with crack length (compliance derivative method). The analysis was performed for various crack-length-to-semi-span ( $a/L$ ) ratios ranging from 0.2 to 0.9. Three material systems representing a wide range of material properties were analyzed. The compliance and strain-energy-release rates of the specimen calculated with the present finite-element analysis agree very well with beam theory equations including transverse shear. The  $G_{II}$  values calculated using the compliance derivative method compared extremely well with those calculated using the virtual crack-closure technique. The  $G_{II}$  values obtained by the compliance derivative method using the top or bottom beam deflections agreed closely with each other. The strain-energy-release

---

\* Research Scientist and Senior Scientist, respectively, Analytical Services and Materials, Inc., Hampton, Va 23666. Work performed under NASA Contract NAS1-18256.

\*\* Senior Scientist, Aerostructures Directorate, U. S. Army Aviation Research and Technology Activity (AVSCOM), NASA Langley Research Center, Hampton, Va 23665-5225.

rates from a plane-stress analysis were higher than the plane-strain values by only a small percentage, indicating that either assumption may be used in the analysis. The  $G_{II}$  values for one material system calculated from the finite-element analysis agreed with one solution in the literature and disagreed with the other solution in the literature.

### INTRODUCTION

With the growing use of laminated composites in aircraft structures, more attention is being paid to the failure modes of such composites. A major source of failure in such materials is delamination (also referred to as a crack in this paper) along ply interfaces. In order to better understand the behavior of laminated composites and to be able to characterize and predict failure, the interlaminar fracture toughness must be evaluated.

ASTM has undertaken a round robin test program to evaluate various test methods for determining the mode II interlaminar fracture toughness of laminated composite materials. The end-notched flexure (ENF) test [1] is being considered for the determination of mode II interlaminar fracture toughness.

The ENF test is a three-point bend test of a unidirectional laminate and is used to obtain the compliance and mode II strain-energy-release rate ( $G_{II}$ ) of the test specimen. A theoretical estimation of the specimen compliance and  $G_{II}$  is useful in correlating and predicting the results of experiments involving different material properties and specimen configurations. For this reason, beam theory equations were proposed in the literature for the ENF specimen [1,2]. The accuracy of these equations

needs to be established by methods which do not use simplifying assumptions of beam theory. Attempts were made to analyze the ENF specimen by two-dimensional finite-element analysis [3-6]. However, the strain-energy-release rates in reference 3 disagreed with those in reference 4 for several values of  $(a/L)$ .

The purpose of this paper is, therefore, to analyze the ENF specimen by finite-element analysis using higher order elements, to determine the specimen compliance and the strain-energy-release rates, and to compare these results with the beam theory solutions. Two methods, virtual crack closure technique (VCCT) and compliance derivative technique, were used to calculate the  $G_{II}$  values. The  $G_{II}$  values calculated from these two methods are compared to each other and to those in references 3 and 4. The analyses were performed for three commonly used material systems for values of delamination length to semi-span  $(a/L)$  ratios ranging from 0.2 to 0.9.

#### SYMBOLS

$a$	crack length
$b$	beam width
$C^{BT}$	beam compliance considering bending deformation
$C^{SH}$	beam compliance considering bending and shear deformation
$C^{FE}$	beam compliance from finite-element analysis $E_{11}, E_{33}$ Young's moduli in x- and y-directions, respectively
$G_{II}^{SH}$	mode II strain-energy-release rate from beam theory considering bending and shear deformation
$G_{13}$	transverse shear modulus

$G_{II}^{FE}$	mode II strain-energy-release rate from finite-element analysis
$h$	beam half-thickness
$L$	beam half-span
$P$	line load
$v^{FE}$	deflection under a unit load calculated using finite-element analysis
$v^{SH}$	deflection under a unit load calculated using beam theory with shear deformation
$\nu_{13}$	Poisson's ratio
$\Delta$	length of the side of a square element around the crack tip

## ANALYSIS

### Specimen Configuration, Loading, and Materials

Figure 1 shows the configuration of the specimen. The specimen is a 24-ply unidirectional laminate with a through-width delamination at mid-depth at one end of the specimen. As shown in the figure,  $a$  is the delamination length,  $L$  is the specimen half-span,  $b$  is the width, and  $2h$  is the thickness. The half-depth,  $h$ , was assumed to be 0.066925 in., and the beam half-span was taken equal to 1.5 in. A line load,  $P$ , is applied at the mid-span as shown in Figure 1.

Three sets of material properties which are shown in Table 1 were considered in this study. Material 1 properties were used to compare the present results with the results of reference 3. Material 2 represents

typical properties for S2/SP250 glass/epoxy, and material 3 represents those of AS4/PEEK.

### Beam Theory Solutions

Simple expressions for compliance and  $G_{II}$  in the ENF test are given in the literature [1,2]. These expressions were obtained by using beam theory with and without shear deformation.

The equation for beam compliance, considering only bending deformation, was given by Russell [1]. For a mid-plane delamination in a unidirectional composite beam, this equation reduces to [5]

$$C^{BT} = \left(1 + 1.5(a/L)^3\right) / \left(4E_{11}b(h/L)^3\right) \quad (1)$$

This equation for  $C^{BT}$  was modified by Carlsson et al. [2] to include the effect of transverse shear deformation

$$C^{SH} = C^{BT} \left[ 1 + \frac{\left(1.2 + 0.9\left(\frac{a}{L}\right)\right)}{\left(1 + 1.5\left(\frac{a}{L}\right)^3\right)} \left(\frac{h}{L}\right)^2 \left(\frac{E_{11}}{G_{13}}\right) \right] \quad (2)$$

The strain-energy-release rates are calculated by taking the derivative of the compliance expression

$$G_{II} = \frac{P^2}{2b} \frac{dC}{da} \quad (3)$$

The  $G_{II}$  values corresponding to compliance Equations (1) and (2),

respectively, are

$$G_{II}^{BT} = (9a^2 P^2) / (16E_{11} b^2 h^3) \quad (4)$$

$$G_{II}^{SH} = G_{II}^{BT} \left( 1 + 0.2 \left( E_{11} / G_{13} \right) (h/a)^2 \right) \quad (5)$$

The compliance and strain-energy-release rate values from these simple expressions will be compared with the finite-element results.

### Finite-Element Analysis

Model. - A two-dimensional plane-strain analysis of the specimen in Figure 1 was performed because the width is large in comparison to the thickness. The difference between plane-strain and plane-stress assumptions will be discussed later in this paper.

Figure 2 shows a finite-element model with 1699 nodes and 516 8-node isoparametric, parabolic elements. A very fine mesh was used in the vicinity of the delamination tip, with square elements around the delamination tip. The same model was used to study the effect of (a/L) ratio on  $G_{II}$ . This was accomplished by moving the support points and the central load point to achieve the desired (a/L) ratio. The (L/h) ratio was the same in all the analyses. A wide range of (a/L) ratios (0.2 to 0.9) and material properties (presented in Table 1) were considered.

Due to transverse loading and an (L/h) ratio of 22.4, the ENF specimen behaves like a plate. Therefore, to examine if reduced integration [7] is needed, all the elements in the model were integrated with three-point-Gaussian quadrature in the two coordinate directions. Then, the analysis was repeated with two-point-Gaussian quadrature. The deflection under the

load and the  $G_{II}$  values calculated by the two quadrature schemes differed by less than 0.1 percent. Therefore, in the rest of the analysis, the two-point-Gaussian quadrature was employed.

Crack-Face Constraints.- Initially, the finite-element model was analyzed allowing nodes on either side of the delamination to deform without any restraint. The resulting deflections indicated that delamination faces had crossed into each other. Because this deformation is physically inadmissible, the nodes along the crack face must be restrained so that such crossover is prevented [3,4]. When such a constraint is prescribed, the delamination faces press against each other and frictional forces will develop along the delamination faces. Thus, in a rigorous analysis, friction needs to be considered. However, the coefficient of friction ( $\mu$ ) needs to be assumed because data on  $\mu$  are not experimentally available. Finite-element analyses were performed in references 4 and 5 for various values of friction,  $\mu$ , and showed that the effect of friction is to lower the  $G_{II}$  values, in general, by a small amount. Therefore, in the present analysis, friction is neglected, i.e., smooth delamination faces are assumed.

In the present analysis, two methods that prevent crossover of the delamination face nodes were used. Figure 3 illustrates these two methods. In the first method, the nodes on either side along the entire delamination face were constrained to move the same vertical distance (i.e., to have the same v-displacement), but were allowed to slide past each other freely (i.e., to have different u-displacements). The nodes on the top and bottom crack face (e.g., g,g') are shown separated in the vertical direction in Figure 3 for clarity only. In the second method, the same constraints as in

the first method were used, but only on a small region of the crack face. Consider the node  $r$  on the crack face vertically above the right support (see Fig. 3). The nodes  $p, q, r, s, t$  belong to two elements, one on either side of node  $r$ . Only these nodes were subjected to multipoint constraints; the remaining nodes on the crack face were unconstrained. The reason for this prescription is that the load transfer from the upper half of the beam to the lower half takes place in a very small region around node  $r$  [5]. Thus, only a few nodes around node  $r$  need to be constrained. The differences in the solutions obtained using the two methods will be discussed later.

Strain-Energy-Release Rates. - The strain-energy-release rates were calculated using Irwin's virtual crack-closure technique. The equations utilized were similar to those given in references 8 and 9.

$$G_I = - \frac{1}{2\Delta} \left[ F_{yi} (v_\ell - v_{\ell'}) + F_{yj} (v_m - v_{m'}) \right] \quad (6a)$$

$$G_{II} = - \frac{1}{2\Delta} \left[ F_{xi} (u_\ell - u_{\ell'}) + F_{xj} (u_m - u_{m'}) \right] \quad (6b)$$

where  $\Delta$  is the element size,  $F_{xi}$  and  $F_{yi}$  are the forces at node  $i$  in the  $x$ - and  $y$ -directions, and  $(u_\ell - u_{\ell'})$  and  $(v_\ell - v_{\ell'})$  are the relative sliding and opening displacements at node  $\ell$ , respectively (see Fig. 4). Forces at node  $j$  and relative displacements between  $m$  and  $m'$  are defined similarly.

A compliance derivative method was also used to obtain the strain-energy-release rates. For each  $(a/L)$  ratio, the finite-element solution yields the deflection under the unit load (and, hence, the compliance) of

the specimen. Using these numerical compliance values for various (a/L) ratios, a curve fit was made to obtain the compliance of the specimen as a function of (a/L) as

$$C = A_1 + A_2(a/L) + A_3(a/L)^2 + \dots \quad (7)$$

where  $A_1$ ,  $A_2$ ,  $A_3$ , etc., are numerical constants determined by a least-square curve fit. The strain-energy-release rate,  $G_{II}$ , was obtained by differentiating Equation (7) and then substituting in Equation (3)

$$G_{II} = \frac{P^2}{2bL} \frac{dC}{d(a/L)} \quad (8)$$

The  $G_{II}$  values by this procedure were obtained using three-, four-, and five-term approximations in Equation (7). Comparison of  $G_{II}$  values indicated a maximum difference of 1.34 percent between the three sets of results. Thus, the cubic polynomial was used in the curve fitting for compliance.

## RESULTS AND DISCUSSION

In this section, various factors that affect the finite-element solution for the ENF specimen are presented first. Then, the compliance and the strain-energy-release rates obtained by the various methods presented earlier are discussed. Next, the present results are compared to the beam theory solutions and other finite-element solutions.

### Multipoint Constraints

The normalized displacements and  $G_{II}$  values (computed by VCCT) obtained for material 1 from the two methods of prescribing multipoint constraints were found to be identical for configurations ranging from very small to very large crack lengths. No overlapping of the crack faces occurred behind the crack tip when the second method was used, indicating the absence of mode I type deformation. Comparison of the two methods confirms that the load transfer from the upper half section of the beam to the lower half occurs in the immediate vicinity of node  $r$  in Figure 3. This was also confirmed by summing the vertical forces at locations  $p$  through  $t$  in the first method and comparing the sum to the support reaction. Similar conclusions were reached in reference 5. The multipoint constraints for the entire crack face (method 1) were used in the rest of this study.

#### Convergence Study

In order to examine the convergence of the finite-element solution, the analysis was first performed using square elements of size 0.0075 in. ( $\Delta/h = 0.112$ ) around the delamination tip. The elements around the delamination tip were then subdivided to obtain element sizes with ( $\Delta/h$ ) values of 0.056 and 0.028 in the two subsequent analyses. Note that this subdivision extends through the specimen thickness and length along narrow bands. Figure 5 shows the convergence of  $G_{II}$  values with mesh refinement for an  $(a/L)$  ratio of 0.4.

The  $G_{II}$  values changed by 1.4 percent as  $(\Delta/h)$  changed from 0.112 to 0.056. For the next refinement, the  $G_{II}$  values changed by 0.5 percent as  $(\Delta/h)$  changed from 0.056 to 0.028. These results indicate that  $G_{II}$  values with  $\Delta/h = 0.028$  can be considered as accurate. Therefore, the model with

$\Delta/h = 0.028$  was used in all subsequent analyses. Converged  $G_{II}$  values at other  $a/L$  ratios are also presented in Table 2 for completeness.

### Specimen Compliance

The deflection under a unit central concentrated load (point D in Fig. 1) equals the compliance of the specimen. The compliance values predicted with the finite-element analyses and those from the shear deformation theory (Eq. (2)) are presented in Table 3. Figure 6 shows typical results for material 1. Excellent agreement is observed between the two sets of results.

### Strain-Energy-Release Rate

In this section, a comparison of strain-energy-release rates,  $G_{II}$ , from two different techniques (VCCT and compliance derivative technique) is presented. The finite-element solutions are also compared with the beam theory solutions and the results in the literature. Finally, the effect of plane-stress and plane-strain assumptions on  $G_{II}$  is examined.

The  $G_{II}$  values calculated by the virtual crack-closure technique (Eq. (6)) and the compliance derivative technique (Eq. (8)) for various materials are given in Table 4, and typical results are shown in Figure 7 for material 1. The  $G_{II}$  values calculated by the two methods are in excellent agreement, showing the consistency of the finite-element results.

Often in experimental investigations, instead of measuring the deflection at the point of load application, some investigators prefer to measure the deflection at a point on the load line but on the bottom surface of the specimen (point D' in Fig. 1). The deflections at point D' will be referred to herein as the bottom deflections. These deflections are also

included in Table 3. The compliance derivative method was also applied to the bottom deflections and the  $G_{II}$  results are included in Table 4. Excellent agreement between  $G_{II}$  values from the compliance derivative technique using either the top or bottom deflections was obtained, indicating that either deflection can be used.

Comparison with Beam Theory Solutions. - In order to assess the usefulness of the beam theory equations in predicting strain-energy release rate, finite-element results for  $G_{II}$  were compared with the beam theory solutions, Equations (4) and (5). These values are included in Table 4. This table and Figure 8 show that the finite-element analysis agrees better with the beam theory with transverse shear than with the theory without shear deformation. The finite-element  $G_{II}$  values, are higher than the shear deformation theory, but the maximum difference is about 7 percent for the range of  $(a/L)$  ratios and materials considered. Note that this maximum difference did not occur at the same  $(a/L)$  ratio for the various materials considered herein. Also, the beam theory neglecting shear deformation gave lower  $G_{II}$  values compared to the finite-element values with larger percentage differences occurring at low values of  $(a/L)$ .

Comparison with Other Solutions from the Literature. - Several finite-element solutions [3-5] of the ENF specimen exist in the literature. The specimen configurations in references 3 and 4 were modeled using 4-node quadrilateral elements. In reference 4, the multipoint constraints were prescribed all along the crack line similar to those in the first method in this study. In reference 3, "nonlinear truss elements" were used to prescribe the constraints along the crack line. In order to have a common basis for comparison, the results shown in Figure 3 of reference 4 and

Figure 7 of reference 3 were normalized with the  $G_{II}^{SH}$  values from Equation (5) and are shown with the results of the present analysis in Figure 9. Note that in references 3 and 4 specimens with different parameters,  $(E_{11}/G_{13})$  and  $L$ , were analyzed. To be able to compare with the results of these references, the present analyses were repeated with the appropriate values of  $(E_{11}/G_{13})$  and semi-span  $L$ . A new finite-element model for  $L = 2$  in. was developed. This model is very similar to that shown in Figure 2 for  $L = 1.5$  in.

The results of the present analysis are in very good agreement with the results of Mall and Kochhar [4] and are in considerable disagreement with the results of reference 3. The disagreement between the present results and reference 3 results is larger for  $(a/L)$  values greater than 0.4. Also, the present results for the two sets of parameters showed very small differences.

Gillespie, et al. [5], presented finite-element results for various values of  $(E_{11}/G_{13})$  and a semi-span,  $L = 1.5$  in. The  $G_{II}$  values presented in reference 5 differed from the shear deformation beam theory by about 2 to 48 percent for  $(E_{11}/G_{13})$  ratios ranging from 12.8 to 26.9. In contrast, in the present analysis, the maximum difference between the finite-element and the shear deformation beam theory is only about 7 percent for  $(E_{11}/G_{13})$  ratios ranging from 10.5 to 31.7. The reasons for these discrepancies are not known.

Plane Stress Versus Plane Strain. - The finite-element analysis in reference 3 was performed assuming plane-stress condition, whereas plane-strain condition was assumed in reference 4. To examine the differences due to these two assumptions, consider the expression for strain-energy-release

rate in Table 6 of reference 10

$$G_{II} = cK_{II}^2 \quad (9)$$

where

$$c = \frac{A_{11}}{\sqrt{2}} \left[ \sqrt{\frac{A_{22}}{A_{11}}} + \frac{2A_{12} + A_{66}}{2A_{11}} \right]^{1/2} \quad (10)$$

for an orthotropic material. The  $A_{ij}$ 's in Equation (10) are the compliance coefficients of the material. The stress-intensity factor  $K_{II}$  is a function of specimen configuration and loading and is identical in plane-stress and plane-strain conditions.

The ratio of  $G_{II}$  for the plane-stress to the plane-strain case is therefore given by the corresponding ratio of  $c$ . This ratio was calculated to be 1.023 for S2/SP250 glass/epoxy (material 2) and 1.016 for AS4/PEEK (material 3). The corresponding ratios from finite-element analysis were obtained as 1.025 and 1.01, respectively.

Since the difference in the plane stress and plane strain results are so small, either assumption may be used in an analysis.

#### CONCLUDING REMARKS

Two-dimensional finite-element analysis of the end-notched flexure specimen was performed using 8-node isoparametric, parabolic elements to evaluate compliance and mode II strain-energy-release rates,  $G_{II}$ . The  $G_{II}$  values were computed using two different techniques: the virtual crack-closure technique (VCCT) and the compliance derivative technique. The analysis was performed for various crack-length-to-semi-span ( $a/L$ ) ratios ranging from 0.2 to 0.9. Three material systems covering a wide range of

material properties were considered. The compliance and  $G_{II}$  values calculated from the finite-element analysis were compared with those based on beam theory equations and with other finite-element solutions from the literature. Based on this analysis, the following conclusions were reached:

1. The compliance of the specimen calculated with the present finite-element analysis agrees very well (within 2.7 percent) with beam theory equations which consider shear deformation. The beam theory with shear deformation underestimates the  $G_{II}$  values in comparison to finite-element results. The maximum difference was about 7 percent. Thus, beam theory equations which include the effect of shear deformation may be used to estimate the compliance and strain-energy-release rates of the end-notched flexure specimen. The results of beam theory equations which do not include the effect of shear deformation differ considerably from the finite-element results, especially at low ( $a/L$ ) ratios.
2. The  $G_{II}$  values were also obtained from the compliance derivative method. The  $G_{II}$  values agreed extremely well (within 1 percent) with those calculated using the virtual crack-closure technique.
3. A close agreement (within 0.3 percent) was obtained between  $G_{II}$  results from the top or the bottom deflections by the compliance derivative method, indicating that either deflection may be used to measure compliance.
4. The strain-energy-release rates from plane-stress analysis are higher than the plane-strain values by about 2.5 percent for S2/SP250 glass/epoxy and 1 percent for AS4/PEEK graphite/thermoplastic.

## REFERENCES

- [1] Russell, A. J.; and Street, K. N.: Factors Affecting the Interlaminar Fracture Energy of Graphite/Epoxy Laminates. Progress in Science and Engineering of Composites, T. Hayashi, K. Kawata, and S. Umekawa, Eds., ICCM-IV, Tokyo, 1982, p. 279.
- [2] Carlsson, L. A.; Gillespie, J. W., Jr.; and Pipes, R. B.: On the Analysis and Design of the End-Notched Flexure (ENF) Specimen for Mode II Testing. Journal of Composite Materials, Vol. 20, Nov. 1986, pp. 594-605.
- [3] Trethewey, B. R., Jr.; Carlsson, L. A.; Gillespie, J. W., Jr.; and Pipes, R. B.: Mode II Interlaminar Fracture During Static and Fatigue Loading. CCM 86-26, Center for Composite Materials, College of Engineering, University of Delaware, Newark, DE.
- [4] Mall, S.; and Kochhar, N. K.: Finite Element Analysis of End-Notched Flexure Specimens. Journal of Composite Technology and Research, Vol. 8, No. 2, Summer 1986, pp. 54-57.
- [5] Gillespie, J. W., Jr.; Carlsson, L. A.; and Pipes, R. B.: Finite Element Analysis of the End-Notched Flexure Specimen for Measuring Mode II Fracture Toughness. Composite Science and Technology, Vol. 27, 1986, pp. 177-197.
- [6] Barrett, J. D.; and Foschi, R. O.: Mode II Stress Intensity Factors for Cracked Wood Beams. Engineering Fracture Mechanics, Vol. 9, 1977, pp. 371-378.
- [7] Zienkiewicz, O. C.: The Finite Element Method. McGraw-Hill, London, 1977.
- [8] Rybicki, E. F.; and Kanninen, M. F.: A Finite Element Calculation of Stress-Intensity Factors by a Modified Crack-Closure Integral. Engineering Fracture Mechanics, Vol. 9, 1977, pp. 931-938.
- [9] Raju, I. S.: Simple Formulas for Strain-Energy Release Rates with Higher Order and Singular Elements. NASA CR-178186, Dec. 1986.
- [10] Fracture Toughness Testing. ASTM STP 381, American Society for Testing and Materials, Philadelphia, PA, 1965.

Table 1 - Material Properties Used in the Present Analysis

	E 11 MSI	E 33 MSI	G 13 MSI	$\nu$ 13
Material 1	16.7	1.4	0.65	0.3
Material 2	6.31	2.5	0.6	0.25
Material 3	21.23	1.5	0.67	0.37

Table 2 - Convergence of  $G_{II}$  Values with Mesh Refinement: (Material 1)

a/L	$G_{II} \times 10^6 \text{ in-lb/in}^2$		
	$\Delta/h = 0.1121$	0.0560	0.0280
0.2	12.9415	13.1274	13.1970
0.4	45.4101	45.9955	46.2033
0.6	97.6077	98.8145	99.2334
0.8	169.368	171.416	172.118
0.9	211.564	214.094	214.959

Table 3 - Comparison of Compliance Values from Finite-Element  
Analyses and Beam Theory Solutions

a/L	FE Analysis		Beam Theory Solution		Percent Difference* $\frac{C^{FE} - C^{SH}}{C^{FE}} \times 100$
	x 10 <sup>5</sup> in-lb	in-lb	x 10 <sup>5</sup> in-lb	in-lb	
	Top of Beam	Bottom of Beam	** BT	*** SH	
Material 1					
0.0	17.8895	17.7610	16.8551	17.8895	0.0
0.2	18.2047	18.0734	17.0574	18.2470	-0.23
0.4	19.8769	19.7484	18.4732	19.8180	0.30
0.6	24.1446	24.0173	22.3162	23.8162	1.36
0.8	32.2045	32.0777	29.7999	31.4550	2.33
0.9	38.0182	37.8909	35.2862	37.0189	2.63
Material 2					
0.0	44.7062	44.5981	44.6087	45.7293	-2.29
0.2	45.3901	45.2820	45.1440	46.4327	-2.30
0.4	49.4907	49.3866	48.8911	50.3480	-1.73
0.6	60.1585	60.0563	59.0619	60.6868	-0.88
0.8	80.5224	80.4211	78.8681	80.6612	-0.17
0.9	95.3141	95.2129	93.3883	95.2654	0.05

Table 3 - ( Continued ).

a/L	FE Analysis		Beam Theory Solution		Percent Difference*
	x 10 <sup>5</sup> in-lb	in-lb	x 10 <sup>5</sup>	in-lb	$C^{FE} - C^{SH}$
	Top of Beam	Bottom of Beam	** BT	*** SH	$C^{FE}$ x100
Material 3					
0.0	14.2584	14.1369	13.2586	14.2622	-0.03
0.2	14.5045	14.3830	13.4177	14.5718	-0.46
0.4	15.8404	15.7217	14.5315	15.8361	0.03
0.6	19.2291	19.1116	17.5544	19.0096	1.14
0.8	25.6082	25.4913	23.4413	25.0470	2.19
0.9	30.1973	30.080	27.7569	29.4379	2.52

\*  $C^{FE}$  is compliance determined from displacement at the top of the beam.

\*\* BT is beam theory considering bending deformation.

\*\*\* SH is beam theory considering bending and shear deformation.

Table 4 - Comparison of  $G_{II}$  Values Calculated by Various Methods

a/L	FE Analysis x 10 <sup>6</sup> in-lb/in <sup>2</sup>			Beam Theory Solution x 10 <sup>6</sup> in-lb/in <sup>2</sup>		Percent Difference*
	VCCT	Compliance Derivative	Compliance Derivative	** BT	*** SH	
		Top	Bottom			
Material 1						
0.2	13.1970	13.2381	13.2399	10.113	12.699	3.77
0.4	46.2033	46.2042	46.2407	40.452	43.038	6.85
0.6	99.2334	99.2827	99.3130	91.017	93.6038	5.67
0.8	172.118	172.474	172.457	161.809	164.395	4.49
0.9	214.959	216.611	216.556	204.789	207.376	3.53
Material 2						
0.2	31.2631	31.1766	31.2102	26.7652	29.5668	5.43
0.4	114.422	114.386	114.435	107.061	109.862	3.99
0.6	249.717	249.846	249.884	240.887	243.688	2.41
0.8	437.108	437.559	437.555	428.243	431.045	1.39
0.9	549.781	551.010	550.975	541.995	544.797	0.91

Table 4 - ( Continued ).

a/L	VCCT	FE Analysis x 10 <sup>6</sup> in-lb/in <sup>2</sup>		Beam Theory Solution x 10 <sup>6</sup> in-lb/in <sup>2</sup>		Percent Difference*
		<u>Compliance Derivative</u> Top	<u>Compliance Derivative</u> Bottom	** BT	*** SH	
						$\frac{\text{FE G II} - \text{SH G II}}{\text{FE G II}} \times 100$
Material 3						
0.2	10.6385	10.5896	10.6133	7.9552	10.4641	1.64
0.4	36.7811	36.8115	36.8468	31.8207	34.3296	6.67
0.6	78.6305	78.7069	78.7311	71.5966	74.1055	5.76
0.8	135.966	136.276	136.266	127.283	129.792	4.54
0.9	169.350	170.938	170.904	161.092	163.601	3.40

\*  $\frac{\text{FE}}{\text{G II}}$  used here is obtained using VCCT.

\*\* BT is beam theory considering bending deformation.

\*\*\* SH is beam theory considering bending and shear deformation.

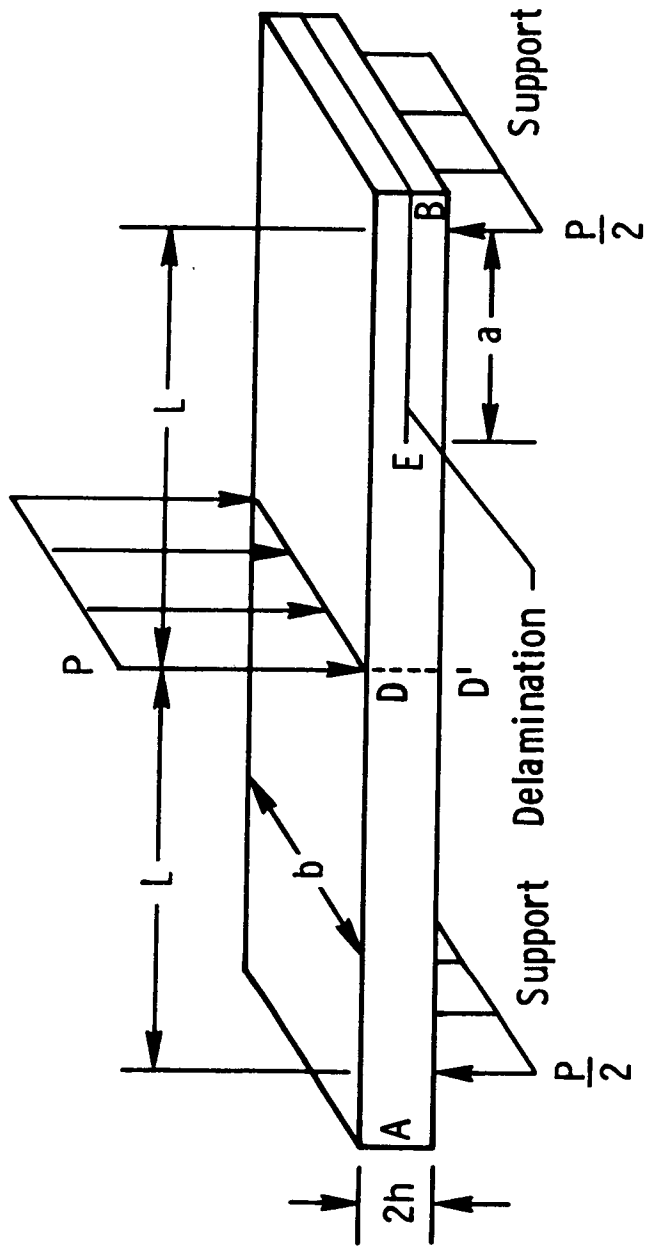


Fig. 1: Specimen configuration and loading.

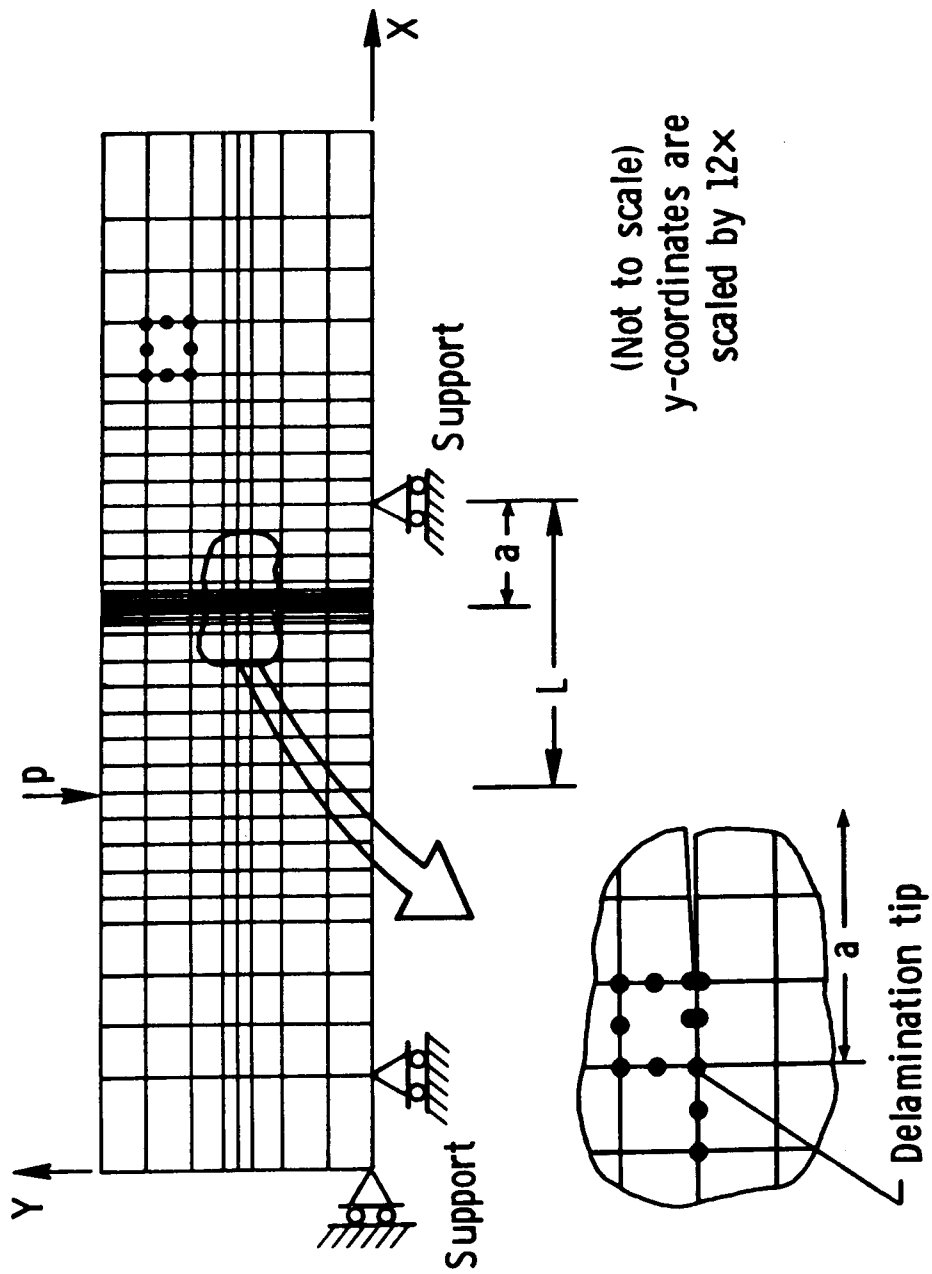
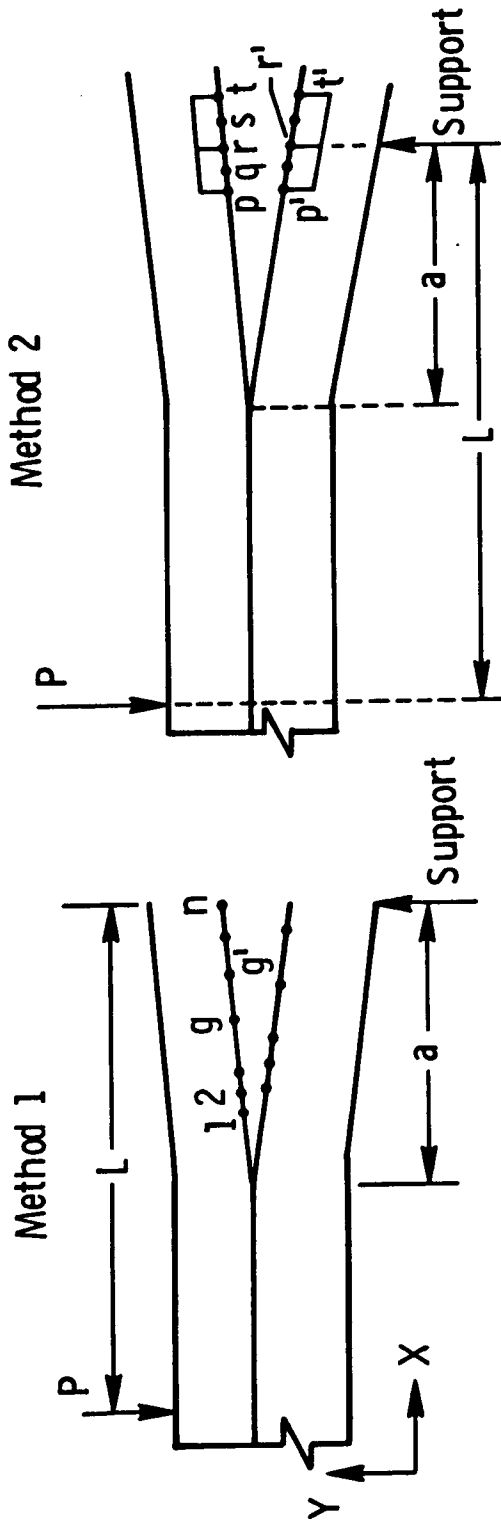


Fig. 2: Finite-element model.

Constraints:  $V_g - V_{g'} = 0$   
 $F_{Y_g} + F_{Y_{g'}} = 0$



Constraints at all nodes  $g = 1, n$

Constraints only at nodes  $g = p, q, r, s$   
and  $t$

Fig. 3: Effect of multipoint constraints.

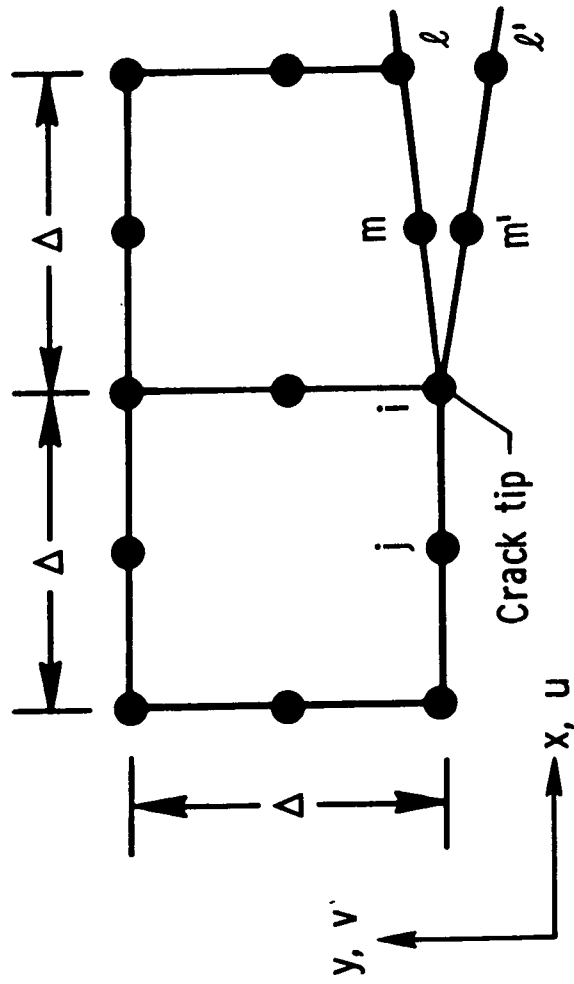


Fig. 4: Detail near the crack tip and nodes used in the strain-energy-release rate calculation.

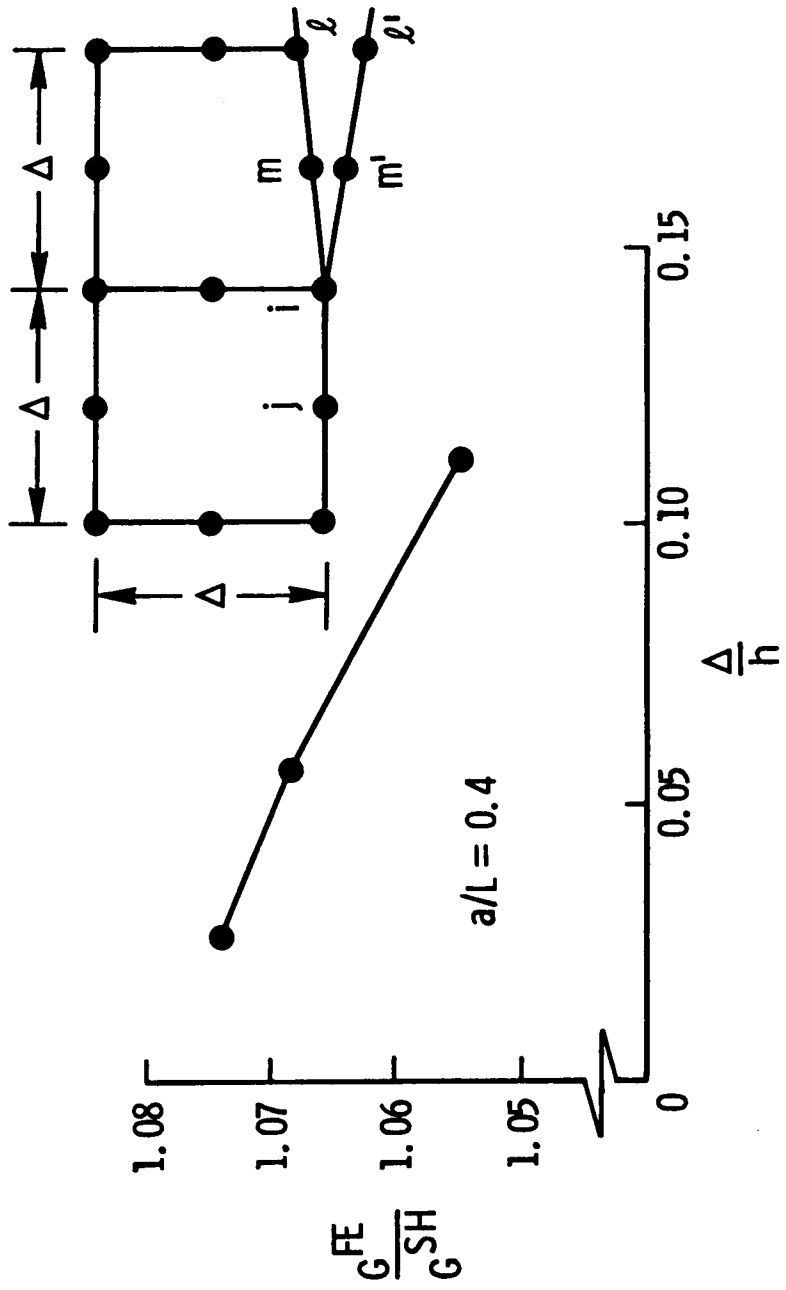


Fig. 5: Variation of normalized  $G_{II}$  calculated using VCCT with mesh refinement.

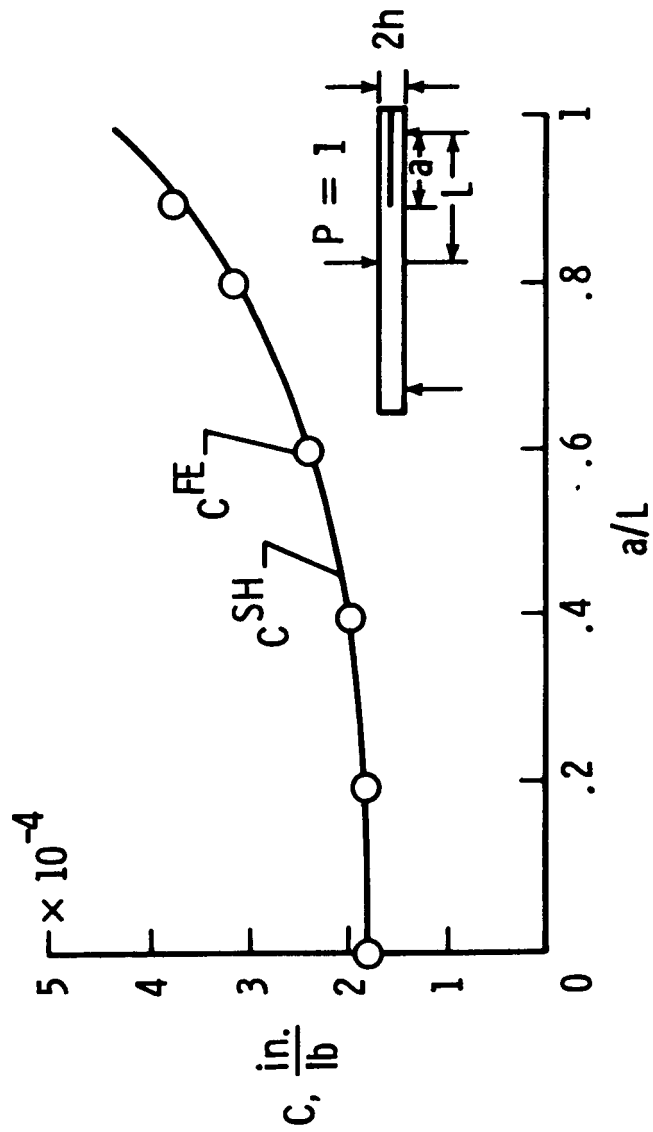


Fig. 6: Comparison of compliance calculated using finite elements and shear deformation beam theory (material 1).

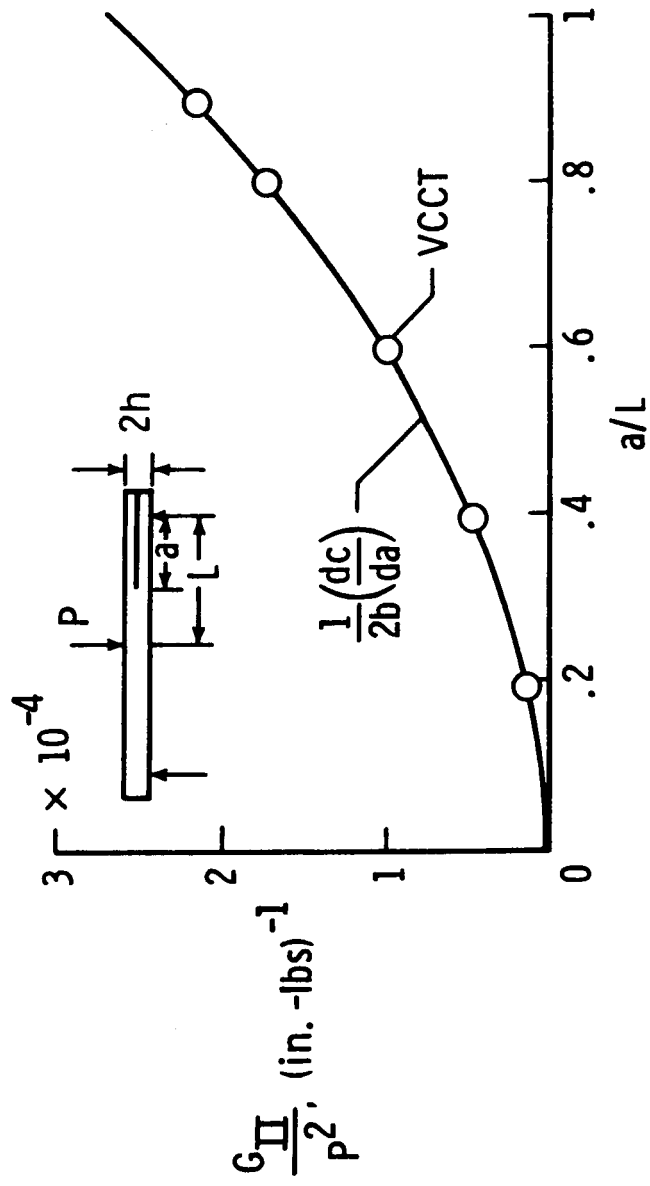


Fig. 7: Comparison of  $G_{II}$  calculated using finite elements by

VCCT and compliance derivative method (material 1).

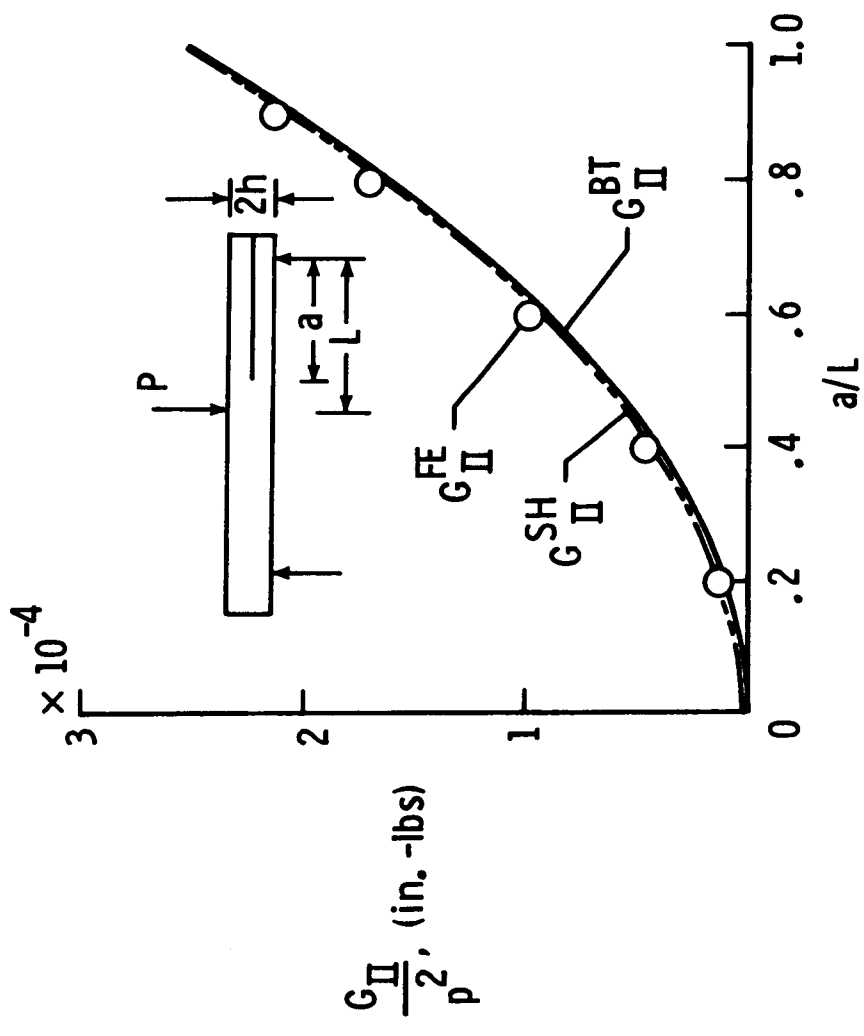


Fig. 8: Comparison of  $G_{II}$  calculated using finite elements and beam theory (material 1).

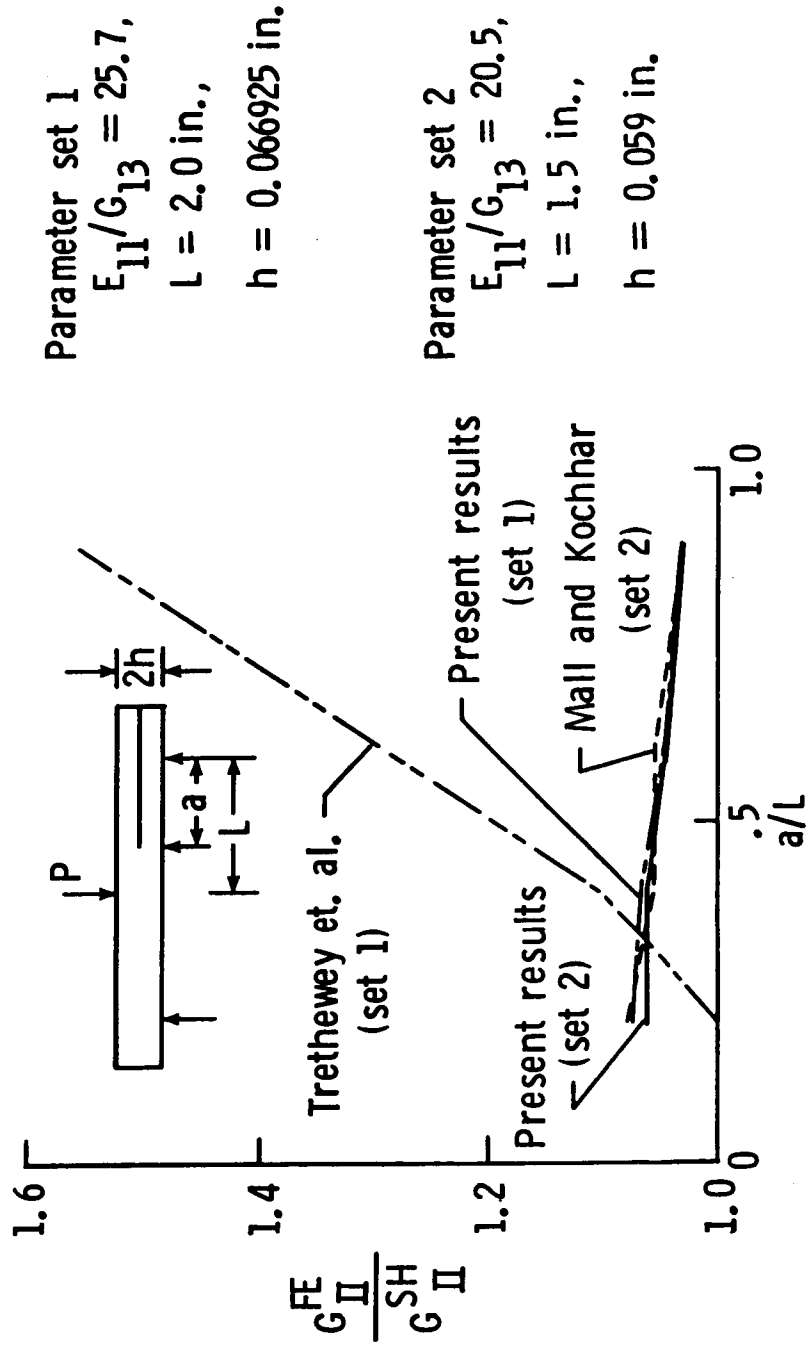


Fig. 9: Comparison of  $G_{II}$  from various analyses.

1. Report No. NASA TM-100494		USAAVSCOM TM 87-B-12		2. Government Accession No.		3. Recipient's Catalog No.	
4. Title and Subtitle Strain-Energy-Release Rate Analysis of the End-Notched Flexure Specimen Using the Finite-Element Method				5. Report Date November 1987			
				6. Performing Organization Code			
7. Author(s) S. A. Salpekar, I. S. Raju, and T. K. O'Brien				8. Performing Organization Report No.			
9. Performing Organization Name and Address NASA Langley Research Center, Hampton, VA 23665-5225 U.S. Army Aviation Research and Technology Activity (AVSCOM), Aerostructures Directorate Hampton, VA 23665-5225				10. Work Unit No. 505-63-01-05			
				Contract or Grant No.			
12. Sponsoring Agency Name and Address National Aeronautics and Space Administration Washington, DC 20546 U.S. Army Aviation Systems Command St. Louis, MO 63166				13. Type of Report and Period Covered Technical Memorandum			
				14. Army Project No.			
15. Supplementary Notes S. A. Salpekar and I. S. Raju, Analytical Services and Materials, Inc., Hampton, VA 23666; T. K. O'Brien, Aerostructures Directorate, USAARTA (AVSCOM), Langley Research Center, Hampton, VA 23665.							
16. Abstract Two-dimensional finite-element analysis of the end-notched flexure specimen was performed using 8-node isoparametric, parabolic elements to evaluate compliance and mode II strain-energy-release rates, $G_{II}$ . The $G_{II}$ values were computed using two different techniques: the virtual crack-closure technique (VCCT) and the rate of change of compliance with crack length (compliance derivative method). The analysis was performed for various crack-length-to-semi-span ( $a/L$ ) ratios ranging from 0.2 to 0.9. Three material systems representing a wide range of material properties were analyzed. The compliance and strain-energy-release rates of the specimen calculated with the present finite-element analysis agree very well with beam theory equations including transverse shear. The $G_{II}$ values calculated using the compliance derivative method compared extremely well with those calculated using the virtual crack-closure technique. The $G_{II}$ values obtained by the compliance derivative method using the top or bottom beam deflections agreed closely with each other. The strain-energy-release rates from a plane-stress analysis were higher than the plane-strain values by only a small percentage, indicating that either assumption may be used in the analysis. The $G_{II}$ values for one material system calculated from the finite-element analysis agreed with one solution in the literature and disagreed with the other solution in the literature.							
17. Key Words (Suggested by Author(s)) End-notched flexure      Delamination Strain-energy release rate Finite-element analysis Fracture mechanics Composites				18. Distribution Statement Unclassified - Unlimited Subject Category 39			
19. Security Classif. (of this report) Unclassified		20. Security Classif. (of this page) Unclassified		21. No. of Pages 32		22. Price* A03	